CLAY MINERALOGY ALONG THE LATERITE PROFILE IN HUBEI, SOUTH CHINA: MINERAL EVOLUTION AND EVIDENCE FOR EOLIAN ORIGIN

HANLIE HONG[1],*, ZHAOHUI LI[1,2], AND PING XIAO[1]

[1] Faculty of Earth Sciences, China University of Geosciences, Wuhan, Hubei, 430074, China
[2] Geosciences Department, University of Wisconsin − Parkside, Kenosha, WI 53141-2000, USA

Abstract—In spite of many studies of laterite origins in various parts of the world, the origin of laterite in the middle to lower reaches of the Yangtze River is still a topic of debate, thus leaving doubts about the prevailing environmental and climatic conditions at the time. The purpose of this study was to provide greater understanding of this subject by examining in more detail the associated mineralogical evolution, *i.e.* clay mineral composition, structural characteristics of clays in various beds with different degrees of weathering along the laterite profile, and the alteration mechanisms during the pedogenic process in tropical to semitropical climate conditions. High-resolution transmission electron microscopy (HTEM), X-ray diffraction, and wavelength dispersive X-ray fluorescence spectrometry were used to characterize the samples in order to link clay mineralogy in various beds with different degrees of weathering along the laterite profile to the formation and origin of laterites in the region. The laterite profile displayed a distinct layered structure and was divided into a saprolite (B4), a light colored net-like clay bed (B3), a brown-red gravelly clay bed (B2), and a dark-brown topsoil (B1), respectively, from bottom to top. The clay mineral assemblage of beds B1 and B2 was illite, kaolinite, and chlorite, while that of beds B3 and B4 was mainly kaolinite with minor illite. The bimodal particle-size distribution of clay minerals in the laterite profile indicated that fine-grained particles could have been produced by partial dissolution and decomposition of coarse-grained ones. Examination by HRTEM revealed that fine-grained particles usually occurred as X-ray amorphous materials in the upper soil beds, but with euhedral morphology in the lower portions, suggesting that the fine-grained particles in the lower soil beds might be partially neoformed during the weathering process. Amorphous spots occurred frequently in kaolinite crystals in the upper soil beds, while the structure of kaolinite was well preserved, with a well defined lattice-fringe image. The illite crystallinity index exhibited a trend of downward decrease, while the values of the chemical index of alteration (CIA = $Al_2O_3/(Al_2O_3+ CaO+ K_2O+ Na_2O) \times 100\%$) of the soil profile showed a trend of downward increase. Samples of the upper soil beds, B1 and B2, had comparable SiO_2/Al_2O_3 ratios of 5.37−6.22, while those of the lower beds, B3 and B4, had significantly smaller SiO_2/Al_2O_3 ratios of 1.92−3.98, suggesting that the latter had a greater degree of weathering than the former, in reasonable agreement with the results of the illite crystallinity and CIA index. In addition, samples from B1 and B2 had similar TiO_2/Al_2O_3 ratios of 0.042−0.053, while those from B3 and B4 had comparable TiO_2/Al_2O_3 ratios of 0.021−0.033, comparable to the value 0.020 of the bedrock, and were notably smaller than the upper soil beds, indicating that materials of the upper soil beds, B1 and B2, had a different origin from the lower soil beds. The upper bed was probably derived from eolian accumulation due to intensification of the winter monsoon and aridity in central Asia and was modified by intense chemical weathering since the late Pleistocene, while the lower bed originated from an *in situ* weathering of the underlying argillaceous limestone.

Key Words—China, Clay Minerals, Eolian Accumulation, Laterite, Weathering.

INTRODUCTION

The mechanism of laterite formation whether by *in situ* weathering, relative or absolute accumulation, or by continual weathering and erosion of a long-exposed landscape is still under debate (Bourman, 1993). In one study, the degree of weathering and differences in clay mineralogy in tropical Costa Rica depended primarily on time (Nieuwenhuyse *et al*., 2000). In another study, the laterite kaolinite was observed in two groups which were high-defect and low-defect, respectively, with the

ordered kaolinite being secondary; the latter might be a useful mineralogical tracer of the recent evolution of old lateritic terrains (Beauvais and Bertaux, 2002).

A large concentration of radiation-induced defects in lateritic kaolinites from Brazil suggested that their chemical, isotopic, and crystallographic properties were inherited from paleoclimates (Balan *et al*., 2005), and an ordered population of the underlying sedimentary kaolinite was gradually replaced by a more recent generation of disordered soil kaolinite from the bottom to the top of the profile (Balan *et al*., 2007). In general, a structural change in defect content was considered as the main characteristic of kaolinite during the lateritization process, and kaolinite might have been replaced by hematite after long-term lateritization. However, petrographic and microprobe studies of clay minerals in an intensely lateritized profile with
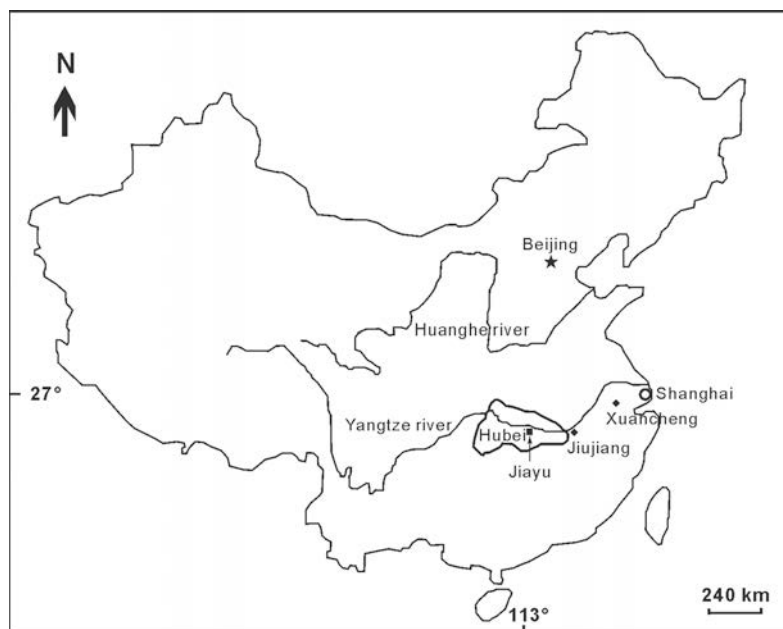
Figure 1. A generalized map showing the location of the study area.

ferricrete duricrusts in central Africa suggested an absolute accumulation of Fe in voids instead of epigenic replacement of kaolinite by hematite (Beauvais, 1999). Previous studies of clay mineral evolution in laterite profiles have suggested that the crystal structure of kaolinite could indicate the weathering process and the amount of structural change could depend on the degree of weathering.

Laterite also occurs widely in south China which has tropical to semitropical climates. Studies of environmental and climatic evolution since the Pleistocene in south China have been mainly focused on investigation of laterite profiles (*i.e*. Zhu, 1993; Zhao and Yang, 1995; Li and Gu, 1997; Hu *et al*., 1998; Xiong *et al*., 2002). However, the formation of laterites in the middle to lower reaches of the Yangtze River has been the subject of debate, making it difficult to establish the environmental and climatic conditions. Based on detailed investigation of laterites, Zhu (1988) suggested that the laterite in the region developed from *in situ* weathering of the underlying argillaceous limestone. On the other hand, studies of a laterite profile in Xuancheng suggested that it was, in fact, the weathering product of eolian deposits, instead of *in situ* weathering, which had occurred since the middle Pleistocene (Zhao and Yang, 1995). Many investigations have focused on stratigraphic characteristics and particle-size analyses, while clay-mineral studies of the laterite profile in the area were rarely undertaken (Hong *et al*., 2009).

In the present study, HRTEM, X-ray diffraction (XRD), and wavelength dispersive X-ray fluorescence spectrometry (WDXRF) were used to characterize the samples taken from the laterite profile.
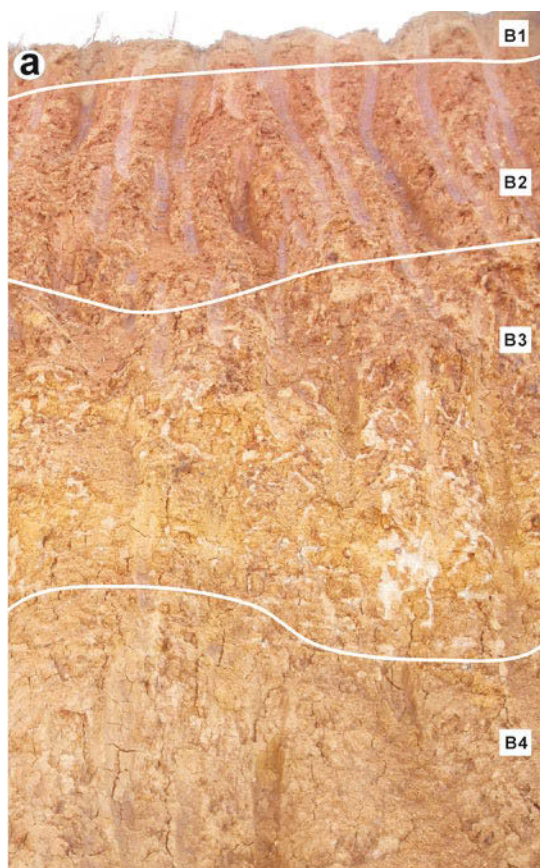

Figure 2. (a *above*) Field photograph of the laterite profile showing the layer structure; (b *facing page*) lithology of the weathering profile.

MATERIALS AND METHODS

The weathering profile and sampling

The laterite profile is located at Jiayu county (113º48′E, 29º51′N), Hubei province, in the middle to lower reaches of the Yangtze River (Figure 1). The climate is warm and humid, with a mean average temperature of ~19ºC and a mean annual rainfall of ~1200 mm, falling mainly between April and October. The landscape is mainly of flat hills covered with evergreen trees and bushes. The hills are undergoing denudation, with accumulation on the valley alluvial plains. Outcrops of bedrock are sporadic while lakes and rivers are common in the area. Recent organic-rich alluvial muds are present locally in the lakes and lowlands between the hills. The altitude ranges from 20 to 80.5 m above sea level, and a typical soil profile occurs on relatively flat hills in the region. In the laterite profile, the bedrock consists of Cambrian to Ordovician argillaceous limestone, and the distinct layered structure is clearly defined by its distinctive color, texture, and composition (Figure 2a,b). Four typical beds developed
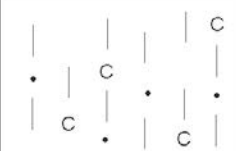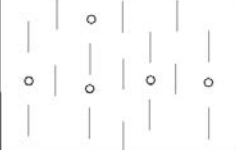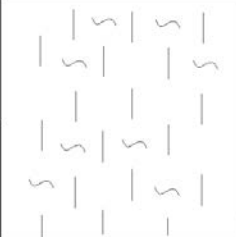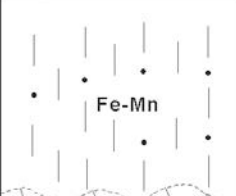
in the weathering profile, which are described briefly from bottom to top as follows.

B4: the saprolite preserves the structure and texture of the parent rock locally. It is a reddish-brown clay layer, while red-brown Fe-bearing nodules and gray-brown Mn-bearing nodules occur locally in this bed.

B3: a light-colored, net-like clay bed (5 to 16 m) is light-yellow, contains net-like white clay veins, and, therefore, exhibits a net-like structure distinct from other beds. The reddish matrix is Fe-enriched relative to the net-like white clay veins.

B2: the brown-red gravelly clay bed above the light-colored net-like clay bed (2 to 5 m thick) contains quartz gravels derived from weathering of silicified limestone and minor Fe and Mn oxides.

B1: the topsoil and the uppermost bed of the weathering profile (0−3 m thick with a mean thickness of ~1 m) is dark-brown and contains ~0.5% organic materials.

The layered structure occurs commonly in laterite profiles in the middle to lower reaches of the Yangtze River. Regional stratigraphic studies of laterite profiles in this area suggested that the light-colored, net-like clay bed was formed during the middle Pleistocene, and the overlying soil beds were formed during the late Pleistocene period (Zhao and Yang, 1995; Li and Gu, 1997). In a laterite profile, the degree of weathering is largely related to the depth of the laterite, and the mineralogy of laterite varies with soil beds along the weathering profile (Fritsch *et al*., 2005). For the clay mineralogical and geochemical investigations in the present study, 15 soil samples were collected from the four soil beds of the laterite profile according to their distinct color, soil texture, and interlayer transitions, and one unweathered bedrock sample was collected from the underlying argillaceous limestone.

Preparation and techniques

Bulk samples were air-dried and then crushed and ground manually to powder grain-size with an agate mortar and pestle. To estimate the mineral composition of the samples, the randomly oriented bulk samples for XRD analysis were prepared by mounting the powder sample onto a sample plate using the back-pressing method. The clay separates were obtained using a sedimentation method described by Jackson (1978), and oriented clay samples for study by XRD were prepared by pipetting the clay suspension onto a glass slide. Ethylene glycol-saturated clay minerals were prepared by treating the oriented samples in a sealed container with ethylene glycol at 65ºC for 4 h to determine whether smectite and/or illite-smectite were present in the samples. To distinguish halloysite from kaolinite, formamide-treated clay separates were prepared using the method proposed by Churchman *et al*. (1984). The slides were allowed to dry at ambient temperature and then sprayed, using a spray bottle, with formamide aerosol for 30 min. The relative abundance of the clay mineral fractions was determined semi-quantitatively by peak heights (I), and was calculated using the formula: $4 \times I$ (illite-10 Å) + $2 \times I$ (kaolinite, chlorite-7 Å) = 100%; the abundances of kaolinite (including minor halloysite) and chlorite were further measured by the intensities of 3.57 Å kaolinite and 3.52 Å chlorite (Biscaye, 1965).

The XRD analysis was performed using a RIGAKU D/MAX-IIIA diffractometer with Ni-filtered CuKα radiation (35 kV, 35 mA) using a 1º divergence slit, a 1º anti-scatter slit, and a 0.3 mm receiving slit. The XRD patterns were recorded from 3 to 65º2θ at a scan rate of 4º2θmin and a resolution of 0.02º2θ. The illite crystallinity index was expressed as the full width at half-height of the (001) reflection, measured from the XRD patterns of the air-dried clay fractions. The XRD patterns of the (02,11) band of kaolinite were collected by the step-scanning method, from 19 to 23º2θ and counting time of 3 s for each 0.02º2θ step.

Chemical analysis was undertaken to estimate the degree of weathering of the soil beds along the laterite profile, based on the chemical index of alteration (CIA = $Al_2O_3/(Al_2O_3+ CaO+K_2O+Na_2O) \times 100\%$) (Nesbitt and Young, 1982). The weight of each sample was ~1 kg, and each was dried in an oven at 60ºC overnight and then ground. The powder sample was pressed to a sample disk using a pressure device (FW-4 model disk maker, Tianjin Tianguang Photic Instrument Co. Ltd., Tianjin City, China). The major-element composition of the samples was obtained using an AXIOS advanced wavelength dispersive X-ray fluorescence spectrometer. The detection limits for major element analysis were 0.01 wt.%.

For HRTEM analysis, the clay separate was immersed in methanol and dispersed with ultrasonic equipment (KH-3200B Model Ultrasonic cleaner, Kunshan Hechuang Ultrasonic Instrument Co. Ltd., Kunshan City, China) for 10 min, collected using a copper net, and then dried under an infrared light. Images and analyses were obtained using a JEM 2010FEF transmission electron microscope operated at 200 kV accelerating voltage and equipped with a Phoenix 60T energy dispersive analytical system.

RESULTS

X-ray diffraction

The XRD investigation of the bulk samples showed that the mineral compositions within the soil beds were relatively uniform, and the notable difference between the soil beds was the occurrence of goethite and chlorite. The XRD patterns of the representative bulk samples of the four soil beds of the laterite profile and the unweathered bedrock sample showed that quartz, kaolinite, and illite were ubiquitous throughout the laterite profile, with slight variations in relative proportions among the beds (Figure 3a). Sample B4 contained significant amounts of goethite, however, while B2 and B1 contained chlorite. Meanwhile, B1 contained 0.65% of organic materials. No shift in peak positions after ethylene glycol solvation indicated that smectite and mixed-layer illite-smectite were absent from the samples.

The XRD patterns of representative clay separates of the four soil beds and their formamide-treated products (Figure 3b) revealed that samples B4 and B3 had similar clay-mineral compositions, consisting mainly of kaolinite and minor illite. Sample B2 consisted mainly of kaolinite and illite, with minor chlorite, while B1 contained mainly kaolinite, illite, and chlorite. Changes in the relative proportions of the clay minerals and of the illite crystallinity were seen along the profile. Similar to the XRD analysis of the bulk samples, the difference in clay mineralogy among the samples was largely defined by the soil beds. The relative abundances of clay minerals in these samples, together with their illite crystallinity values from the upper to the lower

Table 1. Relative proportions of clay minerals (vol.%) and illite crystallinity (IC °2θ) along the laterite profile.

Soil beds	– B1 –		——— B2 ———				——— B3 ———				——— B4 ———				Bed-rock
Sample	15	14	13	12	11	10	9	8	7	6	5	4	3	2	1	rock
Illite	44	47	45	43	46	40	37	25	24	28	22	24	18	16	20	39
Kaolinite	34	28	31	39	44	47	57	75	76	72	78	76	82	84	80	61
Chlorite	22	25	24	18	10	13	6	–	–	–	–	–	–	–	–	–
IC	0.73	0.70	0.68	0.71	0.74	0.72	0.83	0.90	0.96	0.98	0.93	0.88	0.86	0.85	0.80	0.42

sections of the laterite profile (Table 1) indicate that the illite content decreased gradually, while that of kaolinite increased gradually. Chlorite occurred only in B1 and B2.

The intensity of the 10 Å peak of samples B3 and B4 increased slightly, while that of the 7 Å peak decreased slightly after formamide solvation, relative to those of the clay separates. As the 7 Å peak of halloysite (001) expands to 10 Å after formamide treatment (Churchman *et al.*, 1984), the increased intensity of the 10 Å peak and the decreased intensity of the 7 Å peak after formamide solvation could be attributed to intercalation of formamide into the interlayer space of halloysite, thus suggesting the presence of minor halloysite in these samples. However, for samples from B1 and B2, the intensities of the 10 Å and 7 Å peaks were unchanged after formamide solvation, indicating that no halloysite was present in the upper section of the laterite profile.

The XRD results of the (02,11) band of kaolinites (Figure 3c) showed a gradual change in intensities of the $(1\bar{1}0)$ and $(11\bar{1})$ peaks of the samples.

Chemical composition

Samples from B1 and B2 had similar chemical compositions, as did those from B3 and B4 (Table 2). The major differences in chemical composition between the upper and lower sections were the Si and Al contents, and the amounts of mobile elements Mg, Na, and K. The upper section contained significantly more Si with slightly more Ti, Mg, Na, and K, compared to the lower section. The Al contents, on the contrary, were significantly smaller in the upper section.

The Fe content was similar in samples of B1 and B2, notably larger in samples of B4, and remarkably different in those of B3 (Table 2). The abundance of Fe in B3 may be related to reducing conditions and
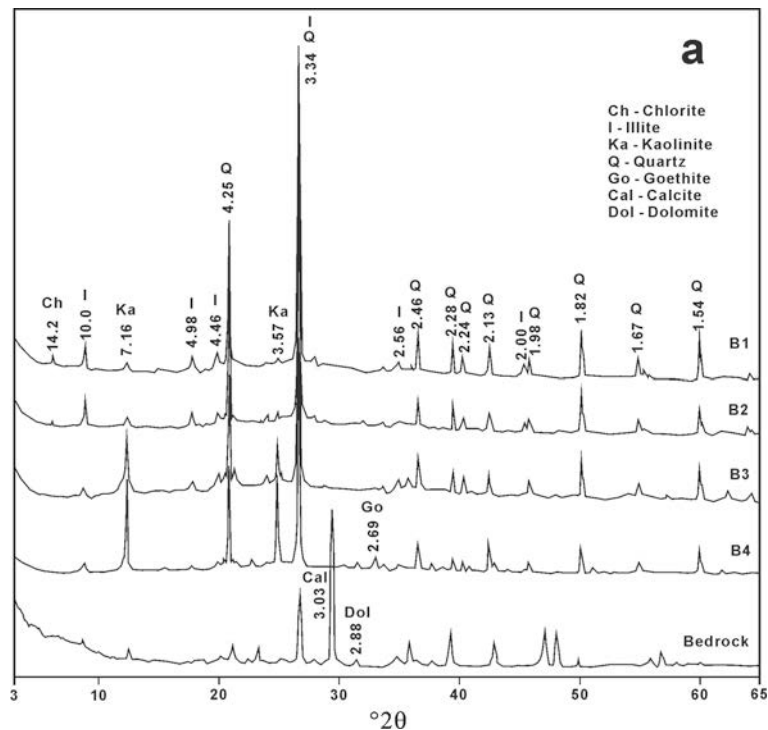

Figure 3 (*above and following two pages*). The XRD patterns of the samples: (a) representative bulk samples of the four beds and the bedrock; (b) clay fractions and clay fractions subjected to formamide; and (c) the (02,11) band of kaolinites showing the change in the crystallinity of kaolinites along the soil profile.

lateral migration under the local hydromorphic conditions.

HRTEM analysis

Examination of the samples by HRTEM revealed no sharp changes in morphology of structure of the clay minerals among samples along the laterite profile, in agreement with the results of the XRD analysis. Variations in the clay mineralogy along the profile could be roughly distinguished by the soil beds. The HRTEM images of the clay minerals in B4 revealed that kaolinite was the most abundant clay mineral, and it exhibited two distinct morphologies. Most of the kaolinite crystals had a relatively larger particle size, with a diameter of 0.2−2 μm in the basal-plane dimension, and exhibited poorly developed hexagonal to pseudo-hexagonal plates with a rounded or irregularly ragged outline. Some of the kaolinite crystals had a

smaller grain size of 0.05−0.2 μm. The latter group of crystals, however, usually displayed euhedral, pseudo-hexagonal morphology (Figure 4a). The basal (001) plane of kaolinite was well developed and appeared smooth or flat, while other surfaces such as (110) and (010) were poorly developed and extremely small, but with edges which were clearly defined. Tubular halloysite crystals were occasionally observed in this bed. Illite was present as elongate, euhedral plates, with straight edges and a regular outline (Figure 4a). The kaolinite structure was generally well preserved as the lattice-fringe image of kaolinite crystals was well defined, with regular, straight lattice fringes (Figure 4b).

Halloysite crystals were frequently observed in B3. They were usually present in curled, tubular, club-like, or multi-layer tubular morphologies (Figure 4c). In general, the tubular or club-shaped halloysite crystals were 0.3−1.2 μm long and 0.1−0.2 μm in diameter. In
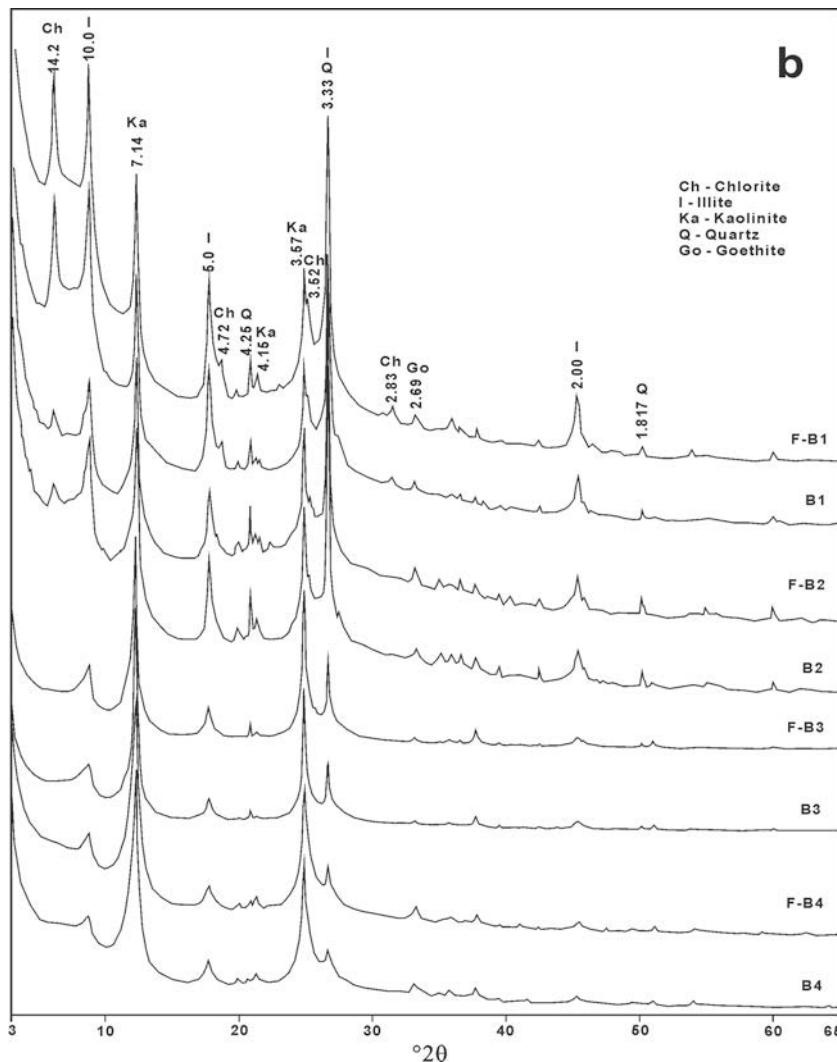

Figure 3 (*contd.*).

Table 2. Elemental composition (reported as oxides) and chemical indices of the laterite profile (wt.%).

Soil beds	Sam-ple	SiO_2	Al_2O_3	Fe_2O_3	TiO_2	MnO	MgO	CaO	K_2O	Na_2O	P_2O_5	LOI	Sum	CIA	SiO_2/Al_2O_3	TiO_2/Al_2O_3
B1	15	72.43	12.48	5.01	0.53	0.01	0.69	0.16	1.61	0.12	0.11	6.74	99.91	86.8	5.80	0.042
	14	69.13	11.77	5.74	0.59	0.13	0.65	0.13	1.70	0.26	0.08	9.32	99.50	84.9	5.87	0.050
B2	13	71.27	13.26	6.25	0.61	0.05	0.56	0.51	1.52	0.11	0.06	5.37	99.43	86.1	5.37	0.046
	12	73.16	12.33	5.68	0.65	0.09	0.67	0.28	1.65	0.27	0.10	5.12	100.0	84.9	5.93	0.053
	11	73.73	11.85	5.84	0.58	0.07	0.63	0.43	1.68	0.25	0.16	4.58	99.80	83.4	6.22	0.049
	10	71.05	12.09	5.35	0.62	0.18	0.55	0.09	1.47	0.17	0.15	8.25	99.97	87.5	5.89	0.051
B3	9	65.28	16.41	7.25	0.54	0.03	0.47	0.30	1.63	0.14	0.12	7.52	99.71	88.8	3.98	0.033
	8	56.61	16.84	4.42	0.41	0.03	0.45	0.27	1.31	0.18	0.16	18.80	99.52	90.5	3.36	0.024
	7	58.47	17.93	2.76	0.39	0.01	0.48	0.21	1.38	0.09	0.07	17.84	99.63	91.4	3.26	0.022
	6	52.12	22.17	8.17	0.48	0.09	0.31	0.10	1.12	0.11	0.07	14.72	99.54	94.3	2.35	0.022
	5	53.20	20.28	7.37	0.52	0.02	0.52	0.23	1.42	0.13	0.07	16.02	99.82	91.9	2.62	0.026
B4	4	49.19	24.43	7.39	0.53	0.19	0.41	0.48	1.61	0.10	0.15	14.86	99.34	91.8	2.01	0.022
	3	48.23	20.99	7.98	0.44	0.17	0.40	0.32	1.53	0.12	0.86	18.55	99.57	91.4	2.30	0.021
	2	42.52	22.13	9.50	0.47	0.04	0.51	0.25	1.34	0.11	0.09	22.06	99.16	92.9	1.92	0.021
	1	51.82	15.71	4.76	0.38	0.05	0.49	0.50	1.54	0.21	1.47	22.98	99.89	88.5	3.30	0.024
Bedrock		28.21	7.49	3.03	0.15	0.09	1.84	28.57	1.23	0.32	0.18	28.08	99.19	19.9	3.77	0.020

* All Fe as Fe_2O_3

LOI: loss on ignition.

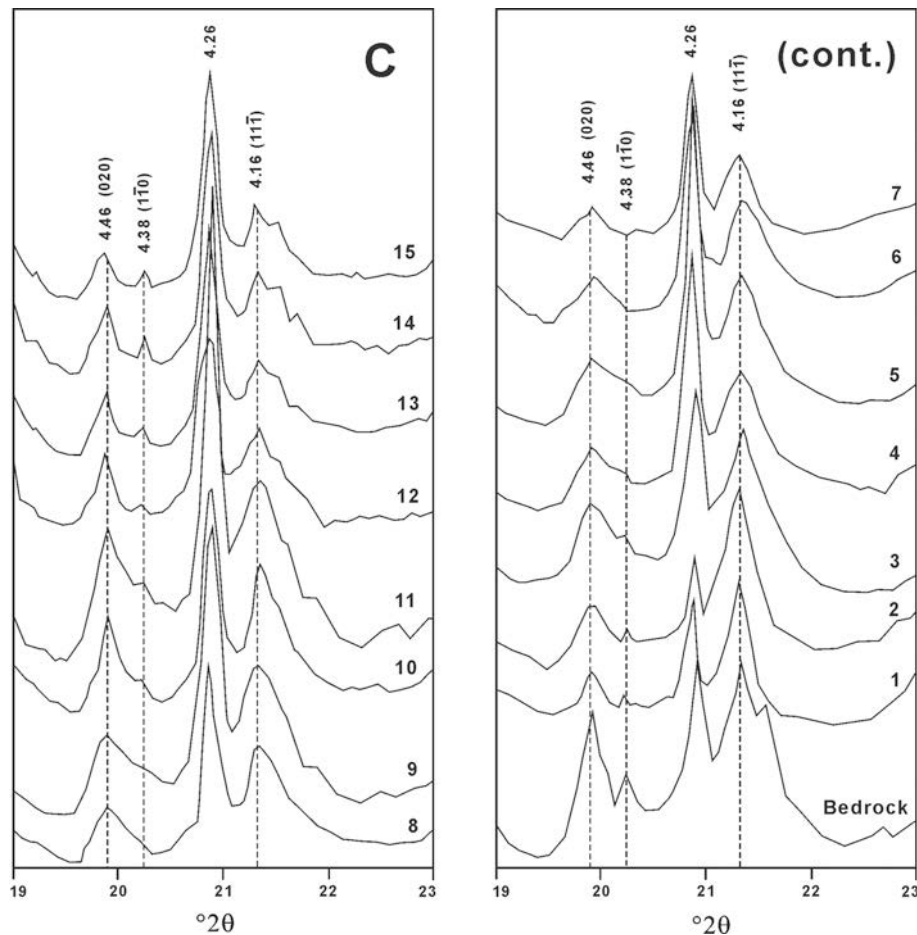CIA: $Al_2O_3/(Al_2O_3 + CaO + K_2O + Na_2O) \times 100\%$

Figure 3 (*contd.*)

addition, very small tubular particles spatially associated with Si, Al concretions were also observed (Figure 4c). In this gel-like material, a tubular crystalline structure was clearly distinguished, by electron diffraction, from the nearby amorphous Si, Al concretion, indicating that halloysite crystallized from the gel-like material
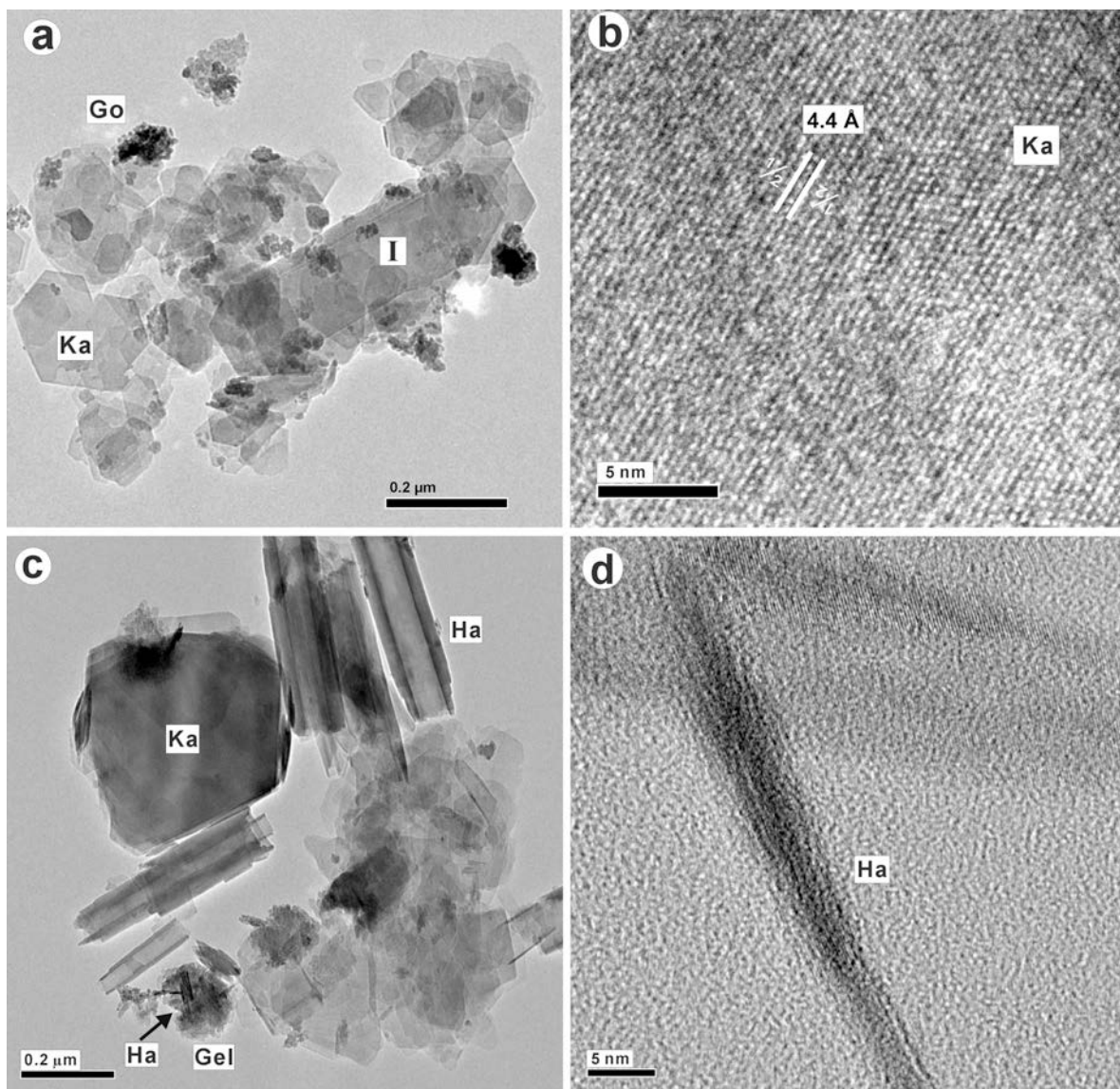

Figure 4 (*above and following two pages*). (a) HRTEM image of clay minerals of the reddish-brown clay (B4) showing euhedral morphology for the fine-grained particles; (b) lattice-fringe image of kaolinite crystals of bed B4 showing that the kaolinite structure was generally well preserved in this horizon. The fringe spacing, 4.4 Å, is consistent with the (020) diffraction of kaolinite in the direction perpendicular to the (001) surface. (c) Tubular halloysite in the light-colored, net-like clay (B3) sample as curled, tubular, club-like, or multi-layered tubular morphologies. The tubular particles crystallized from gel-like materials. (d) Lattice-fringe image of the tubular crystal, as in Figure 3c, showing that the structure was well defined in amorphous Si, Al concretions and confirming crystallization of halloysite from gel-like materials. (e) Clay particles of bed B3 exhibit thinned and irregular, ragged edges, and the basal (001) plane of kaolinite appears uneven. (f) Kaolinite of bed B2 displaying blurred lattice fringes; decomposition took place along the (001) surface at the edges of kaolinite. (g) Gel-like materials observed in bed B1. (h) In bed B1, a kaolinite particle was coated by Fe (oxyhydr)oxides or surrounded by an Fe-rich mass; illite crystals exhibited elongated plates with ragged edges. (i) Lattice-fringe image of a kaolinite crystal showing well developed amorphous spots in a kaolinite crystal of bed B1. (j) In bed B1, a relict illite grain with well defined lattice fringes surrounded by amorphous materials at the crystal margin. The 4.5 Å spacing of the fringe is consistent with the (110) surface of illite, and the Si/Al ratio and K are in agreement with the chemical composition of illite. (k) Chlorite exhibiting an irregular outline in bed B1; the chemical composition of Si, Al, Mg, Fe, and K is consistent with chlorite.

(Figure 4d). Unlike the morphology of the kaolinite crystals in B4, kaolinite crystals in B3 usually had thinned and irregular, ragged edges, and the basal (001) plane appeared uneven. Abundant small and thin particles with ragged edges were observed, while euhedral pseudo-hexagonal grains were only occasionally found in this sample (Figure 4e). The kaolinite structure was similar to that of B4. However, both the needle-like Fe oxide particles and the tubular halloysite grains clearly exhibited lattice fringes.

Both kaolinite particles and amorphous materials were frequently observed in the sample of B2. Kaolinite crystals exhibited a rounded outline, and the (001) surface was uneven and of variable thickness, regardless of its particle size. The rounded edges and the uneven surfaces were characteristic of dissolution. Tubular halloysite crystals and elongate illite plates were only occasionally found in the sample. The lattice fringes of kaolinite crystals appeared progressively blurred, and the thinned edges illustrated the decomposition of small plates along the (001) surface of kaolinite at the edges (Figure 4f).

The clay mineral particles in B1 had been decomposed more intensely. Thin and small (nm-sized) clay particles occurred commonly in the sample. This type of clay particle displayed a ragged outline. Gel-like
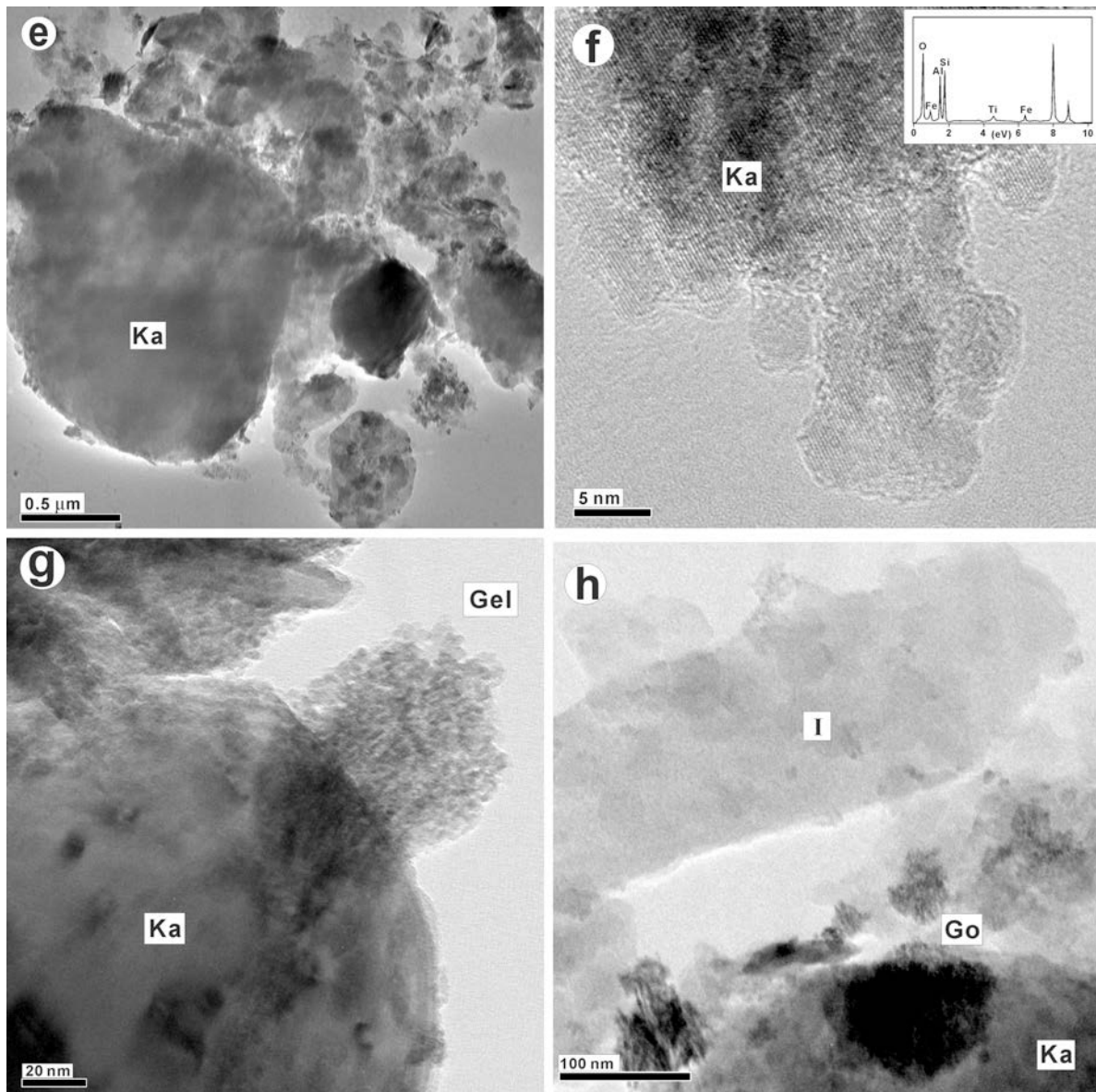

Figure 4. (*contd.*)

materials were also observed commonly in the sample (Figure 4g). The larger clay particles exhibited well developed, uneven (001) surfaces, while amorphous spots were frequently observed in clay particles. Iron (oxyhydr)oxides occurred more abundantly in other beds and were in close association with clay particles. Some of the clay particles were coated with the Fe (oxyhydr)-oxide phase or surrounded by an Fe-rich mass with well developed needles (Figure 4h). The well developed amorphous spots in kaolinite crystals appeared to favor their decomposition into much smaller grains (Figure 4i).

Illite and chlorite particles were frequently observed in B1. Illite crystals usually showed elongate plates with ragged edges (Figure 4h), suggesting intense dissolution. The lattice fringes of illite crystals appeared to be blurred, and at the margins of the particles, small illite relics with well defined illite lattice fringes were surrounded by amorphous materials (Figure 4j). Chlorite usually exhibited an irregular outline (Figure 4k), similar to that of illite. Decomposition took place at the crystal edges. Amorphous spots occurred frequently in chlorite crystals, and in particular, fine-grained relict chlorite particles surrounded by
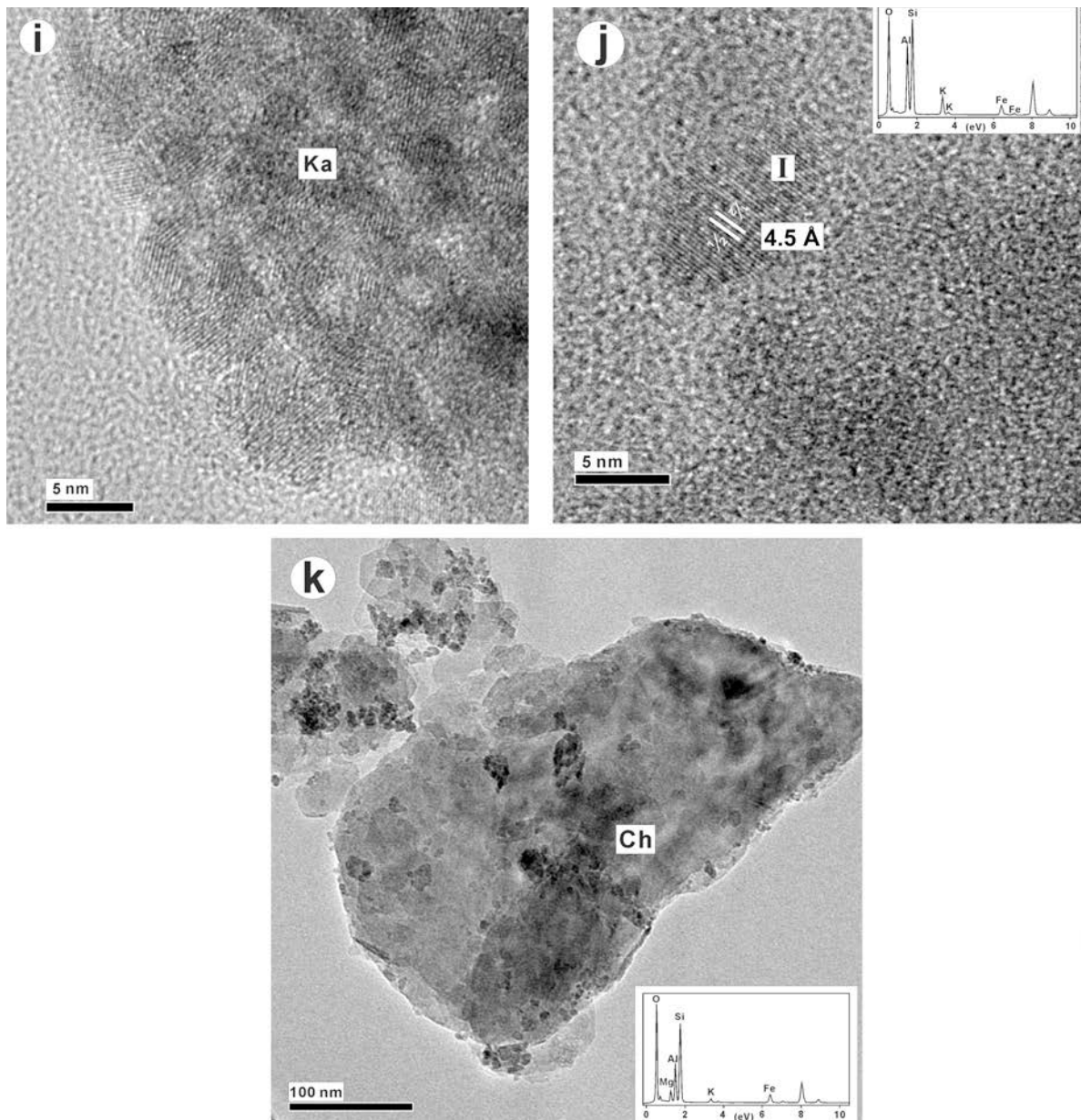

Figure 4. (*contd.*)

amorphous materials were observed at the margins of the larger particles.

Both kaolinite and illite particles were frequently observed in the bedrock. Analogous to those in B4, illite was usually present as elongate plates, and kaolinite usually appeared as pseudo-hexagonal grains, with relatively straight edges and regular outlines. The lattice-fringe images of kaolinite exhibited similar characteristics to that of B4, with regular, straight lattice fringes.

DISCUSSION

Chemical weathering indices of the beds

During the lateritization process, mobile elements would be lost and immobile elements would be enriched relative to the composition of the underlying, unweathered rock. The samples of the upper two soil beds were remarkably enriched in Si (Table 2). Compared to the upper section, the notable enrichment of Al, together with the smaller concentrations of mobile elements such as Mg, Na, and K in beds B3 and B4 suggested that more intense depletion occurred in the lower section than in the upper one.

The CIA index reflected the accumulation of the immobile element Al and the depletion of mobile elements Ca, K, and Na, and, therefore, characterized the weathering intensity within a weathered soil profile (Nesbitt and Young, 1982; Nedachi *et al.*, 2005). The CIA values of the soil samples along the profile fell into two groups (Table 2). Samples of B1 and B2 had similar CIA values of 83.4−87.5%, while those of B3 and B4 had similar CIA values of 88.5−94.4%, indicating different degrees of weathering between the upper and lower sections of the laterite profile and a smaller degree of weathering in the upper section relative to the lower section. However, compared to the CIA value of 19.9% for the bedrock, all samples of the soil profile had notably larger CIA values, suggesting intense chemical weathering of these materials, in agreement with the XRD results. Analogous to the CIA index, samples of the beds B1 and B2 had similar SiO_2/Al_2O_3 values of 5.37 to 6.22, while samples of the lower beds, B3 and B4, had significantly smaller SiO_2/Al_2O_3 ratios of 1.92 to 3.98. The lesser depletion of Si in the upper section compared to the lower section also indicated a smaller degree of weathering in the upper part of the soil profile.

In an *in situ* weathering profile, the TiO_2/Al_2O_3 ratio would remain relatively constant in soil horizons with different degrees of weathering (Nesbitt and Young, 1982; Nedachi *et al.*, 2005). In the present study, however, samples of the upper soil beds, B1 and B2, had similar TiO_2/Al_2O_3 ratios of 0.042−0.053, significantly larger than those of 0.021−0.033 for the lower soil beds, B3 and B4, which were comparable to the value of 0.020 for the bedrock. Therefore, the distinct TiO_2/Al_2O_3 ratios between the upper and the lower

sections suggest that the upper soil beds had a different origin from the lower section, which were not derived from *in situ* weathering of the underlying bedrock.

Origin of materials in the laterite profile

The bedrock of the weathering profile consisted mainly of argillaceous limestone, which contained significant amounts of the precursor clay minerals. Previous study of the formation of the light-colored net-like clay in the laterite profile suggested that the materials were related to the underlying argillaceous limestone (Hong *et al.*, 2009). However, the HRTEM and XRD analyses reported here illustrated the heterogeneity of the clay mineralogy from the different soil beds along the weathering profile, arguing against an homogeneous origin of the soil beds.

Illite has been described as a little-altered detrital mineral derived from the pre-existing bedrock, and chlorite was a common mineral of greenschist-grade metamorphic rocks and some sedimentary rocks (Weaver, 1989). Illite and chlorite are characteristic of cold regions and deserts, and the clay mineral assemblage of illite and chlorite is an indicator of immature soils which had undergone little chemical weathering (Robert and Kennett, 1994). Kaolinite formed during the warm and wet weathering of acidic igneous and metamorphic rocks or their detrital weathering products, and the occurrence of kaolinite in soil profiles would indicate intense weathering under possible tropical conditions (Hallam *et al.*, 1991).

During pedogenesis in which chemical weathering dominated, chlorite would transform into kaolinite or smectite, and in laterite soils, chlorite would be completely eliminated after intense weathering and was only limited to fresh bedrock (Vicente *et al.*, 1997). In permanently humid tropical red or yellow lateritic soils, therefore, the typical paragenesis is quartz, kaolinite, and goethite (Tardy and Nahon, 1985). In the weathering laterite profile of Hubei, however, chlorite occurred abundantly in samples of the uppermost soil bed and decreased gradually downward. No chlorite was observed in the lower section of the laterite profile or in the bedrock (Table 1). The incongruent clay mineral assemblage between the upper and lower sections suggests that the upper section had a different origin from the lower section, in good agreement with the chemical analysis, and the occurrence of chlorite is clearly indicative of an eolian origin for the upper part of the profile.

In weathering profiles, illite is a common product of weathering reactions with low hydrolysis; the high illite crystallinity is attributed to the minimum hydrolyzation in cold/dry climatic conditions and, on the contrary, the lower illite crystallinity is attributed to intense hydrolyzation in warm/humid conditions (Chamley, 1989). Although, illite could be ubiquitous along weathering profiles under temperate to tropical climate conditions,

as a result of progressive weathering reactions, illite would show a downward increase in crystallinity as the weathering front moved downward, illite in the upper section experienced more prolonged weathering in comparison with the lower section. However, the XRD results (Table 1) showed that from the upper to lower parts of the laterite profile, the illite crystallinity indices exhibited a decreasing trend downward, indicating much more intense weathering of illite in the lower than in the upper section.

In a study of the laterite profile at Jiujiang, near this soil profile, Xiong et al. (2002) showed that the lower section exhibited more intense weathering than the upper section based on geochemical index calculations, in good agreement with the clay evidence for the laterite profile. Previous studies on laterite gold deposits in the area showed that gold occurred mainly in B4 in the lower sections of the laterite profile, which was derived from weathering of the underlying gold-mineralized bedrock (Hong, 2000; Hong and Tie, 2005), confirming that deep, in situ chemical weathering had taken place in the region. Chemical indices of the soil beds suggested, however, that the upper section was not derived from weathering of the lower beds. In the middle to lower reaches of the Yangtze River, formation of laterite profiles was modified with eolian accumulation during the late Pleistocene, which was in chronological correspondence with the increasing loess accumulation in northwestern China (Xiong et al., 2002). The comparable clay mineral assemblage of illite, chlorite, and kaolinite between the upper section of laterite profiles in south China and the paleosols of the eolian loess sequences in northwestern China also indicated an eolian origin of the materials. As suggested by Sun and Wang (2005), the enhancement of Asian monsoons for the past ~3 Ma has resulted in a more widespread accumulation of Plio−Pleistocene loess in China. The accumulation of eolian materials in the middle to lower reaches of the Yangtze River during the period probably resulted from intensification of the winter monsoon and aridity in central Asia, which may have been caused by global cooling (Miller et al., 2005).

Mineralogical evolution along the weathering profile

Changes in physico-chemical conditions during the weathering process would result in mineralogical evolution along the profile. In general, clay minerals in the weathering profile could be divided into two particle-size groups, i.e. the fine-grained and the coarse-grained (HRTEM observation, Figure 4e). The existence of a bimodal particle-size distribution in the weathering profile suggested that small particles may have been formed by partial dissolution of larger ones (Vicente et al., 1997). Comparing clay morphologies of samples along the laterite profile, both kaolinite and illite clearly exhibited more euhedral morphologies in the lower section (Figure 4a,c) than in the upper section

(Figure 4h). On the contrary, fine-grained materials with thin, small particle dimensions occurred commonly in the upper section. In B4, kaolinite crystals with relatively large particle sizes usually displayed poorly developed hexagonal to pseudo-hexagonal morphology, while those with smaller particle sizes usually exhibited euhedral, pseudo-hexagonal crystals. However, kaolinite particles, regardless of size, exhibited a remarkable change in morphology from euhedral to anhedral in an upward direction through the profile. In B1, the larger kaolinite crystals had irregular or rounded edges and uneven (001) surfaces. Amorphous spots occurred frequently in the crystals and smaller kaolinite particles usually occurred as amorphous materials (Figure 4g), suggesting that dissolution, rather than formation, of kaolinite occurred in the upper horizons.

In the crystal structure of kaolinite, small amounts of Fe can replace Al, and the increase in Fe content could result in reduction in the crystallinity and in the degree of order of kaolinite (Brindley et al., 1986; Balan et al., 1999). Mineralogical studies of laterites in tropical Amazonia and Africa indicated that in evolving weathering profiles, kaolinite commonly exhibited a progressive upward increase in Fe content and decrease in kaolinite crystallinity, corresponding to an increasing abundance of defects in kaolinite crystals (Fritsch et al., 2005). The defect structure of kaolinite could be assessed from the (02,11) band in the XRD pattern, which was estimated from the ratio of the sum of the heights of the peaks $(1\bar{1}0)$ and $(11\bar{1})$ measured from the inter-peak background to the height of the $(1\bar{1}0)$ peak measured from the general background (Hinckley, 1963). A decrease in crystallinity would result in a decrease in resolution of neighboring peaks and an increase in the inter-peak diffraction intensity, and an increase in the frequency of defects would decrease the absolute intensity of the $(1\bar{1}0)$ peak (Plançon et al., 1988).

Kaolinites in the uppermost and lowermost sections had more intense $(1\bar{1}0)$ peaks relative to those in the middle of the laterite profile (Figure 3c), decreasing gradually from sample 15 of B1 to sample 7 of B3 and then increasing gradually to sample 1 of B4, suggesting more structural defects and thus a deeper weathering of kaolinites in B3 compared to the other soil beds, in agreement with the HRTEM observations. The poor resolution of the (02,11) band of kaolinites in all beds, however, showed a significantly smaller degree of crystallinity relative to that of the bedrock (Figure 3c). An intense chemical weathering is suggested for the laterite profile. The more developed structural defects of kaolinite in the lower section suggested a deeper weathering relative to that in the upper section. Differences in kaolinite crystallinity between the lower and upper sections probably reflect the differences in their origins.

In weathering profiles of temperate to tropical environments, intense oxidation and lixiviation could

result in a near-neutral groundwater, which would in turn increase the solubility of Si and Al, in particular, and increase the activity of Fe^{3+}, thus favoring the incorporation of Fe^{3+} in the kaolinite structure and leading to the poor crystallinity of kaolinite in the environment (Hong and Tie, 2005). Observations by HRTEM also revealed that well developed amorphous spots occurred commonly in larger kaolinite crystals in the laterite profile, and the larger particles exhibited decomposition along the edges (Figure 4f,i), indicating that intense weathering resulted in the decomposition of larger clay particles.

Crystallization of tubular halloysite particles from gel-like materials was also observed in B3 (Figure 4c,d). Rapid groundwater movement and water activity favored the formation of halloysite (Keller, 1978), as this bed was situated just above the groundwater table in the weathering profile. As indicated by the representative XRD patterns of clay fractions of B3 and B4 (Figure 3b), changes in intensity of the 10 Å and 7 Å peaks after formamide treatment suggested the occurrence of halloysite in these beds, consistent with the HRTEM observations.

In weathering profiles, alteration of kaolinite could produce halloysite, while dehydration of halloysite could produce kaolinite due to long-term weathering, which depends on the local kinetic processes (*i.e.* humidity, redox, lithology, and fissuring) during weathering (Churchman and Gilkes, 1989; Stumm, 1992; Bobos *et al.*, 2001). As the weathering proceeded, surficial zones were gradually lost to dissolution, transformation, and/or erosion, and dissolution of materials in the upper sections could have produced soluble Si and Al, which would accumulate in the lower sections due to downward movement of groundwater, and the concentrations of Si and Al would gradually increase with weathering (Fritsch *et al.*, 2005). Colloids of SiO_2 and Al_2O_3 usually crystallize as kaolinite and halloysite, when the concentrations of Si and Al are large enough for crystallization of kaolin phases, which would have deposited in the lower sections of the weathering profile, and therefore, the small, euhedral kaolinite particles in the lower sections might have been partially neoformed during the weathering process, in good agreement with the HRTEM observation, suggesting that dissolution and crystallization were attributed to clay mineralogy in the laterite profile during the weathering process, and decomposition of larger kaolinite particles was also the cause of the bimodal particle-size distribution. Whether kaolinite formation corresponds to present-day weathering conditions in the profile, or if its occurrence is related to some past processes, is unclear.

CONCLUSIONS

Both the CIA and SiO_2/Al_2O_3 indices of the samples fell into two groups: samples of the upper soil beds, B1 and B2, had similar CIA values of 83.4−87.5%, while samples of the lower soil beds, B3 and B4, had comparable CIA values of 88.5−94.4%. Analogous to the CIA index, samples of the upper beds B1 and B2 had comparable SiO_2/Al_2O_3 ratios of 5.37 to 6.22, while samples of the lower beds, B3 and B4, had significantly smaller SiO_2/Al_2O_3 ratios of 1.92−3.98, comparable to that of 3.77 of the bedrock, suggesting that the upper section experienced a smaller degree of weathering than the lower section of the laterite profile. Samples of the upper section had similar TiO_2/Al_2O_3 ratios of 0.042−0.053, and samples of the lower section had comparable TiO_2/Al_2O_3 ratios of 0.021−0.033, comparable with the value 0.020 of the bedrock and notably lower than the upper soil beds, suggesting different origins for the two sections. The upper soil beds, B1 and B2, were probably derived from eolian accumulation modified by intense chemical weathering during the late Pleistocene, while the lower soil beds, B3 and B4, originated from *in situ* weathering of the underlying argillaceous limestone. Therefore, laterites in the middle to lower reaches of the Yangtze River were produced by *in situ* weathering combined with modification of the eolian accumulation.

In the laterite profile, the clay mineral assemblage of the upper section was illite, kaolinite, and chlorite, while that of the lower section was mainly kaolinite with minor illite. The occurrence of chlorite also indicated an eolian origin for the upper part of the profile. Clay particles occurred roughly in two particle-size groups and the bimodal distribution suggested that small particles could have been formed by partial dissolution of larger particles, and the small, euhedral kaolinite particles in the lower sections may have been partially neoformed during the weathering process.

In the upper soil beds, the coarse-grained kaolinite crystals exhibited irregular or rounded edges and uneven (001) surfaces, and the fine-grained kaolinite particles usually occurred as amorphous materials. Well developed amorphous spots in kaolinite crystals occurred commonly in the upper beds, which favored the decomposition of kaolinite particles. In the lower soil beds, kaolinite displayed a more euhedral morphology than that in the upper beds, though kaolinite of B3 exhibited a smaller degree of crystallinity, suggesting more structural defects in kaolinite and, therefore, deeper chemical weathering of B3 in the profile.

REFERENCES

Balan, E., Allard, T., Boizot, B., Morin, G., and Muller, J. P. (1999) Structural Fe^{3+} in natural kaolinites: new insights from electron paramagnetic resonance spectra fitting at X and Q-band frequencies. *Clays and Clay Minerals*, **47**, 605−616.

Balan, E., Allard, T., Fritsch, E., Selo, M., Falgueres, C., Chabaux, F., Pierret, M.C., and Calas, G. (2005) Formation and evolution of lateritic profiles in the middle Amazon basin: Insights from radiation-induced defects in kaolinite. *Geochimica et Cosmochimica Acta*, **69**, 2193−2204.

Balan, E., Fritsch, E., Allard, T., and Calas, G. (2007) Inheritance *vs.* neoformation of kaolinite during lateritic soil formation: a case study in the middle Amazon Basin. *Clays and Clay Minerals*, **55**, 253−259.

Beauvais, A. (1999) Geochemical balance of lateritization processes and climate signatures in weathering profiles overlain by ferricretes in Central Africa. *Geochimica et Cosmochimica Acta*, **63**, 3939−3957.

Beauvais, A. and Bertaux, J. (2002) In situ characterization and differentiation of kaolinites in lateritic weathering profiles using infrared microspectroscopy. *Clays and Clay Minerals*, **50**, 314−330.

Biscaye, P.E. (1965) Mineralogy and sedimentation of recent deep-sea clays in the Atlantic Ocean and adjacent seas and oceans. *Geological Society of America Bulletin*, **76**, 803−832.

Bobos, I., Duplay, J., Rocha, F., and Gomes, C. (2001) Kaolinite to halloysite-7 Å transformation in the kaolin deposit of São Vicente de Pereira, Portugal. *Clays and Clay Minerals*, **49**, 596−607.

Bourman, R.P. (1993) Perennial problems in the study of laterite − a review. A*ustralian Journal of Earth Sciences*, **40**, 387−401.

Brindley, G.W., Kao, C.C., Harrison, J.L., Lipsicas, M., and Raythatha, R. (1986) Relation between structural disorder and other characteristics of kaolinites and dickites. *Clays and Clay Minerals*, **34**, 239−249.

Chamley, H. (1989) *Clay Sedimentology*. Springer-Verlag, Heidelberg, Germany, 623 pp.

Churchman, G.J. and Gilkes, R.J. (1989) Recognition of intermediates in the possible transformation of halloysite to kaolinite in the weathering profiles. *Clay Minerals*, **24**, 579−590.

Churchman, G.J., Whitton, J.S., Claridge, G.G.C., and Theng, B.K.G. (1984) Intercalation method using formamide for differentiating halloysite from kaolinite. *Clays and Clay Minerals*, **32**, 241−248.

Fritsch, E., Morin, G., Bedidi, A., Bonnin, D., Balan, E., Caquineau, S., and Calas, G. (2005) Transformation of haematite and Al-poor goethite to Al-rich goethite and associated yellowing in a ferralitic clay soil profile of the middle Amazon Basin (Manaus, Brazil). *European Journal of Soil Science*, **56**, 575−588.

Hallam, A., Grose, J.A., and Ruffell, A.H. (1991) Paleoclimatic significance of changes in clay mineralogy across the Jurassic-Cretaceous boundary in England and France. *Palaeogeography, Palaeoclimateology, Palaeoecology*, **81**, 173−187.

Hinckley, D.N. (1963) Variability in ''crystallinity'' values among the kaolin deposits of the coastal plain of Georgia and South Carolina. *Clays and Clay Minerals*, **11**, 229−235.

Hong, H.L. (2000) Behaviour of gold in the weathered mantle at Shewushan, Hubei, China. *Journal of Geochemical Exploration*, **68**, 57−68.

Hong, H.L. and Tie, L.Y. (2005) Characteristics of the minerals associated with gold in the Shewushan supergene gold deposit, China. *Clays and Clay Minerals*, **53**, 162−170.

Hong, H.L., Li, Z., Yang, M.Z., Xiao, P., and Xue, H.J. (2009) Kaolin in the net-like horizon of laterite in Hubei, south China. *Clay Minerals*, **44**, 51−66.

Hu, X.F., Yuan, G.D., and Gong, Z.T. (1998) Origin of Quaternary red clay of southern Anhui province. *Pedosphere*, **8**, 267−272.

Jackson, M.L. (1978) *Soil Chemical Analysis*. Published by the Author, University of Wisconsin Madison, USA.

Keller, W.D. (1978) Kaolinization of feldspars as displayed in scanning electron micrographs. *Geology*, **6**, 184−188.

Li, C. and Gu, Y. (1997) Stratigraphic study on the vermicular red earth at Xiushui county, Jiangxi province. *Journal of Stratigraphy*, **21**, 226−232 (Chinese text with English abstract).

Miller, K.G., Kominz, M.A., Browning, J.V., Wright, J.D., Mountain, G.S., Katz, M.E., Sugarman, P.J., Cramer, B.S., Christie-Blick, N., and Pekar, S.F. (2005) The Phanerozoic record of global sea-level change. *Science*, **310**, 1293−1298.

Nedachi, Y., Nedachi, M., Bennett, G., and Ohmoto, H. (2005) Geochemistry and mineralogy of the 2.45 Ga Pronto paleosols, Ontario, Canada. *Chemical Geology*, **214**, 21−44.

Nesbitt, H.W. and Young, G.M. (1982) Proterozoic climates and plate motion inferred from major element chemistry of lutites. *Nature*, **299**, 715−717.

Nieuwenhuyse, A., Verburg, P.S.J., and Jongmans, A.G. (2000) Mineralogy of a soil chronosequence on andesitic lava in humid tropical Costa Rica. *Geoderma*, **98**, 61−82.

Plançon, A., Giese, R.F., and Snyder, R. (1988) The Hinckley index for kaolinite. *Clay Minerals*, **23**, 249−260.

Robert, C. and Kennett, J.P. (1994) Antarctic subtropical humid episode at the Paleocene-Eocene boundary: clay-mineral evidence. *Geology,*, **22**, 211−214.

Stumm, W. (1992) *Chemistry of the Solid-Water Interface*. J. Wiley, New York, 428 pp.

Sun X.J. and Wang, P.X. (2005) How old is the Asian monsoon system? − Palaeobotanical records from China. *Palaeogeography, Palaeoclimatology, Palaeoecology*, **222**, 181−222.

Tardy, Y. and Nahon, D. (1985) Geochemistry of laterites, stability of Al-goethite, Al-hematite, and Fe^{3+}-kaolinite in bauxites and ferricretes: an approach to the mechanism of concentration formation. *American Journal of Science*, **285**, 865−903.

Vicente, M.A., Elsass, F., Molina, E., and Robert, M. (1997) Palaeoweathering in slates from the Iberian Hercynian Massif (Spain): investigation by TEM of clay mineral signatures. *Clay Minerals*, **32**, 435−451.

Weaver, C.E. (1989) *Clays, Muds, and Shales*. Developments in Sedimentology, **44**, Elsevier, Amsterdam, 819 pp.

Xiong, S.F., Sun, D.H., and Ding, Z.L. (2002) Aeolian origin of the red earth in southeast China. *Journal of Quaternary Science*, **17**, 181−191.

Zhao, Q. and Yang, H. (1995) A preliminary study on red earth and changes of Quaternary environment in south China. *Quaternary Sciences*, **15**, 107−115 (Chinese text with English abstract).

Zhu, J.J. (1988) Genesis and research significance of the plinthitic horizon. *Geographical Research*, **7**(4), 12−20 (Chinese text with English abstract).

Zhu, X.M. (1993) Red clay and red residuum in south China. *Quaternary Sciences*, **13**, 75−84 (Chinese text with English abstract).